

ORIGINAL RESEARCH




Experimental study of the thermal performance of spiral flow solar water heating system

Ahmed Abdulsitar, Mechanical Engineering Department, College of Engineering, University of Zakho, Duhok, Kurdistan Region 42002, Iraq

Nofal Hasan, Mechanical Engineering Department, College of Engineering, University of Mosul, Mosul 41200, Iraq

Ali Basem, Air Conditioning Engineering Department, Faculty of Engineering, Warith Al-Anbiyaa University, Karbala 56001, Iraq

Ahmed Daabo  and **Hudhaifa Hamzah**, Mining Engineering Department, College of Petroleum and Mining Engineering, University of Mosul, Mosul 41200, Iraq

Abdulelah Yaseen, Department of Petroleum Engineering, College of Engineering, Al-Kitab University, Kirkuk 36015, Iraq

Address all correspondence to Ahmed Daabo at ahmeddaboo@yahoo.com

(Received: 20 February 2024; accepted: 3 July 2024)

ABSTRACT

- *Evaluating the flow rate influence on the spiral collector.*
- *Comparing the thermal efficiency of a spiral collector with a changing flow rate.*
- *Highlighting the influence of some factors on the spiral collector's performance, such as wind speed, solar irradiance, and water inlet temperature.*

The Iraqi population experiences a scarcity of hot water during the winter season. In this paper, the utilization of solar collectors emerges as a viable alternative to conventional sources of energy, such as electricity and fuel, and Solar Water Heating Systems (SWHS) are widely regarded as a viable alternative for water heating, particularly in regions where the cost of fuel and electricity is high or where access to these resources is limited. The analysis of the collector's performance was conducted by considering the variables of solar irradiance, wind speed, and mass flow rate. A maximum overall heat loss coefficient was $5.36 \text{ W/m}^2 \text{ }^\circ\text{C}$ and a maximum useful heat gain was 505 W. The study revealed a positive correlation between solar irradiance, water mass flow rate, and the performance of the collector. Conversely, a negative relationship was observed between wind speed and the collector's performance. The experiment revealed that the spiral collector achieved a maximum efficiency of 66.3%, with a flow rate of 0.042 kg/s. Additionally, the spiral collector demonstrated a maximum increase in water tank temperature of $23.3 \text{ }^\circ\text{C}$, at mass flow rates of 0.042 and 0.05 kg/s.

Keywords sustainability · thermal conductivity · water · glass · energy storage

Discussion

- The efficacy of governmental subsidies for solar water heating systems, particularly in low-income and developing regions, poses inquiries on the fair and equal availability of long-lasting technology.
- The significance of cultural views and customer behavior in the acceptance of solar water heating systems emphasizes the necessity of tackling society's attitudes toward renewable energy technologies.
- The influence of domestic manufacturing capabilities and supply chains on the cost efficiency and environmental friendliness of solar water heating systems is still a substantial and unresolved matter.

Introduction

Renewable energy represents a viable and ecologically conscious substitute for non-renewable energy resources. Solar energy is widely recognized as a significant form of renewable energy due to its capacity to generate electricity¹⁻³ and provide water heating capabilities. Water heating devices in residential settings are responsible for a substantial portion of energy consumption, accounting for approximately 20% of the overall energy usage within households.⁴ To tackle this matter, researchers have developed SWHS that harness solar radiation to convert it into thermal energy for water heating. The provision of hot water in the Kurdistan region of Iraq poses a significant challenge during the winter season, primarily due to the predominant reliance on electricity and gas as the primary energy sources for water heating. Balamurali and Natarajan⁵ carried out a study that focused on the development of a suitable heat transfer fluid (HTF) and the incorporation of internal grooves into the HTF ducts to optimize the performance of flat-plate concentrator, utilizing Mumbai, a peak global radiation of 800 W/m² and an ambient temperature of 32.5 °C, as the location for investigation. Evaluation of the thermophysical properties of three different base fluids—Molten Salt, Dowtherm A, and Therminol VP-1—indicated that Therminol VP-1 exhibited superior performance, with specific heat, density, and thermal conductivity values of approximately 1688.8 J/kg-K, 1351.6 kg/m³, and 20.99 W/mK, respectively, at 50 °C. Furthermore, an assessment of three distinct internal groove configurations (plain, rectangular, and trapezoidal) demonstrated that the trapezoidal profile enhanced system efficiency, resulting in an outlet temperature of 51.6 °C and a useful heat gain of 1478 W. The efficiency of the trapezoidal profile (77.3%) surpassed that of the plain and rectangular groove profiles by 1.01% and 1.003%, respectively. Moreover, the experimental data for the LFPC system utilizing water and a plain duct were documented for comparison with other configurations.

The utilization of SWHS can serve as a viable solution for the provision of hot water by harnessing renewable energy sources. The utilization of SWHS has experienced consistent growth in popularity, as evidenced by the global adoption of this system by over 70 million households in the year 2010.⁶ By the conclusion of the year 2020, the implementation of SWHS has been observed in no less than 134 nations across the globe, resulting in the production of approximately 501 GW of thermal energy.⁶ The classification of SWHS can be divided into two distinct categories: direct systems and indirect systems. In direct solar thermal systems, the circulation of water occurs within a collector that is directly exposed to sunlight. Conversely, indirect solar thermal systems employ a heat transfer fluid to convey heat from the collector to a storage tank. Both direct and indirect systems employ a pump to facilitate the circulation of the fluid. Nevertheless, there exist certain variations of SWHS that eliminate the need for a pump, such as the thermosiphon system. This particular system harnesses the force of buoyancy to facilitate the

circulation of the fluid.⁷ SWHS can also be classified according to the method of heat absorption. Solar heat absorption is a widely employed practice that involves the utilization of two primary methods: active systems and passive systems.⁸ A new receiver with homogenizer and spiral was suggested in Ref. 9 to enhance thermal efficiency by reducing thermal deformation of the absorber tube. A plane structure homogenizer improves the solar flux uniformity through second reflection. The optical-thermal efficiency of the PTC was enhanced by the spiral and homogenizer combination. A three-dimensional model was initially used to study the collector's performance. Results indicate over 96% reduction in thermal deformation and 1.2%–0.63% improvement in optical-thermal efficiency compared to conventional receivers. The proposed receiver effectively reduces thermal deformation and enhances optical-thermal efficiency. There are many types of solar collectors which have been studied and utilized in various applications.¹⁰ Nasir et al.¹¹ conducted a practical experiment to investigate the impact of mass flow rate on a Flat Plate Collector (FPC) in Babylon, Iraq. The experiment involved the utilization of five distinct mass flow rates, specifically 0.14 kg/s, 0.21 kg/s, 0.28 kg/s, 0.35 kg/s, and 0.42 kg/s, respectively. In the conducted experiment, a plastic absorber with a length of 17.4 m was utilized. The glass employed had a thickness of 3.5 mm, while the collector's area measured 2.4 m². The findings indicated that the system attained optimal efficiency when operating at a mass flow rate of 0.35 kg/s. Singh et al.¹² examined thermal performance of a solar collector with water and Cu-MWCNTs nanofluid. Nanoparticles were characterized using X-ray diffraction and FESEM with EDAX mapping. Experimental setup varied flow rates, inclination angles, volume concentrations, and intensity. A 3D numerical model of the flat-plate collector was created using Fluent/Ansys software. SST turbulence model captured changes in velocity, temperature, and pressure fields. Experimental results showed 79.74% efficiency improvement at specific conditions. The maximum deviation between experimental and numerical data was 3.5% for temperature. Numerical data deviated by 2.8% and 2.9% for efficiency and heat gain. The current and voltage output of contaminated SPV modules exhibited a decrease in comparison to their clean counterparts as the droppings functioned as an obstruction to sunlight, thus diminishing power generation and efficiency.¹³ The Engineering Equation Solver (EES) software was utilized to conduct an analysis of the FPC in Mosul, Iraq, employing three distinct materials as the heat absorber. Copper, aluminum, and carbon steel plates were employed as heat absorbers. The objective of the study was to determine the optimal material for enhancing and maximizing the efficiency of the FPC (Flexible Printed Circuit). Copper demonstrated greater efficacy in water heating, while carbon steel exhibited comparatively lower effectiveness in this regard.¹⁴ Maldonado et al.¹⁵ conducted an empirical investigation on the FPC in order to assess the performance of SWHS in the specific environmental conditions of Mexico. The area of the plate absorber was 1.4 m², while the storage tank had a capacity of

100 L. The experimental data were collected over the course of a single day. During the course of the experiment, the highest recorded temperature of the water contained within the storage tank reached 55 °C. Subsequently, a decrease in temperature of 7 °C was observed during the nocturnal period. Various flow rates were employed in the experiment, ranging from 0.0038 kg/s to 0.04 kg/s. The system achieved optimal efficiency when operating at its maximum flow rate.

A practical experiment was conducted in Tanzania to investigate the impact of glass thickness on fracture propagation characteristics FPC. Four distinct glass thicknesses were utilized, measuring 3 mm, 4 mm, 5 mm, and 6 mm, respectively. The research conducted revealed that the highest level of efficiency was attained with a glass thickness of 4 mm, whereas the lowest level of efficiency was observed with a glass thickness of 6 mm.¹⁶

The previous mentioned studies highlight the importance of conducting the current work, as there are no similar studies that have raised similar works. So, the investigators carried out a series of experiments on solar collectors, all of which consistently exhibited exceptional thermal efficiency. Serpentine flow flat-plate solar collectors were predominantly employed by the researchers, rather than spiral flow flat-plate solar collectors. The research utilized the spiral flow methodology to examine the influence of different mass flow rates on the efficiency of a spiral flow solar collector. The primary objective was to ascertain the most suitable mass flow rate for this particular scenario. Given the scarcity of research on solar collectors in our region, the present investigation was conducted.

This research endeavors to evaluate the thermal effectiveness of a spiral flow collector as a prospective alternative to traditional energy sources in mitigating the scarcity of hot water during the winter season in Iraq. The investigation was conducted in Duhok, a city situated in the north of Iraq. It is widely acknowledged that Iraq possesses abundant solar energy resources. Solar technologies are infrequent and costly in Iraq. The study introduces a domestically manufactured solar collector that proficiently heats water and is appropriate for household applications. The goal is to assess the influence of mass flow rate on the

thermal performance of the spiral collector and recommend the optimal mass flow rate for this specific context.

Theoretical framework of heat transfer in the context of solar collectors

Energy balance of the flat-plate collector

Flat-plate collector is a solar collector that is designed to gather solar radiation and transform it into thermal energy, as depicted in Fig. 1. The quantity of thermal energy generated by the FPC represented as Q_i , can be quantified using Eq. (1).¹⁷

$$Q_i = IA. \quad (1)$$

Equation (2) considers the solar irradiance (I) and the surface collector area (A) when calculating the amount of heat energy generated by FPC. Nevertheless, it should be noted that not all solar radiation that reaches the plate can pass through the glass cover, and it is possible that the absorber plate may not fully absorb all of the heat. To incorporate these factors, the transmittance of the glass cover (τ) has a value of 0.89, and the absorptivity (α) of the plate, with a value of 0.81, is included in Eq. (2). The value of τ is determined by the thickness and angle of the glass in the collector, while α is determined by the material and color of the plate.

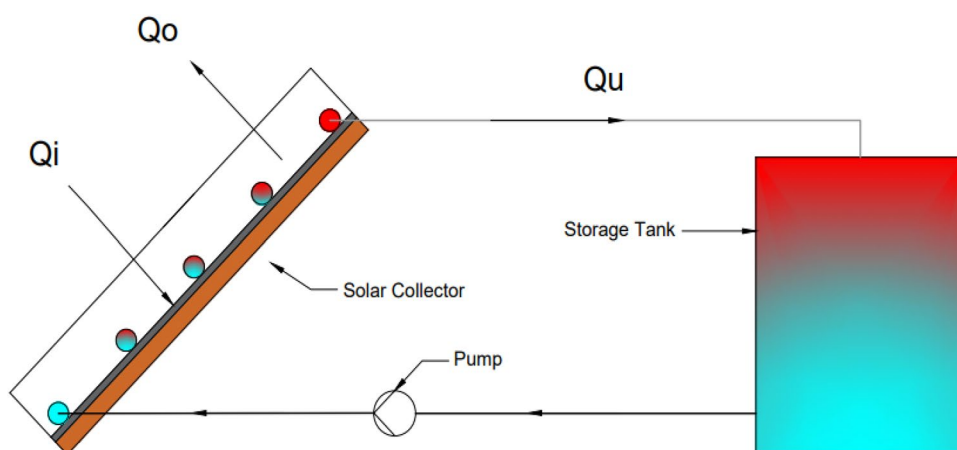
$$Q_i = (\tau\alpha)IA. \quad (2)$$

A portion of solar radiation is reflected by the absorber plate, leading to heat dissipation Q_0 from the FPC to the surrounding environment in instances where the absorber plate is at a higher temperature than the ambient temperature. The quantification of heat loss can be achieved by utilizing Eq. (3), in which U_L represents the overall heat coefficient, T_p denotes the plate temperature, and T_a signifies the ambient temperature.

$$Q_0 = U_L A (T_p - T_a). \quad (3)$$

Once the calculations for Q_i and Q_0 have been performed, it becomes possible to determine the useful heat of the collector, denoted as Q_U . This denotes the quantity of thermal energy that

Figure 1. Schematic drawing of the spiral flow solar water heating system.



is accessible for utilization or retention. The value of Q_U can be determined by utilizing (4).¹²

$$Q_U = Q_i - Q_0,$$

$$Q_U = (\tau\alpha)IA - U_L A(T_p - T_a). \quad (4)$$

The estimation of Q_u can be conducted by utilizing (5) the thermal energy of the working fluid as it traverses through the collector.¹⁸⁻²⁰

$$Q_u = \dot{m}C_p(T_o - T_i). \quad (5)$$

The fluid outlet temperature is denoted as T_o , while the fluid inlet temperature is represented by T_i . The mass flow rate is symbolized as m , and the specific heat capacity is denoted as C_p . Equation (6) presents the heat removal factor as the ratio of Q_u to Q_U , which is commonly referred to as the Hottel-Whillier equation.

$$F_R = \frac{\dot{m}C_p(T_o - T_i)}{(\tau\alpha)IA - U_L A(T_i - T_a)}. \quad (6)$$

Equation (7) can be utilized to calculate the thermal efficiency of the collector.

$$\eta = \frac{\int Q_u dt}{\int Q_i dt},$$

$$\eta = F_R \tau \alpha - F_R U_L \left(\frac{T_i - T_a}{I} \right), \quad (7)$$

where U_L represents the overall heat transfer coefficient and can be determined by utilizing the following formula:

$$U_L = U_T + U_B + U_E. \quad (8)$$

The top loss coefficient is denoted as U_T , the bottom loss coefficient as U_B , and the edge loss coefficient as U_E .

Top loss coefficient (U_T)

The value of U_T can be determined by utilizing the next equation:

$$U_T = \left[(h_1 + h_2)^{-1} + (h_3 + h_4)^{-1} + (h_5)^{-1} \right]^{-1}. \quad (9)$$

The heat lost through convection from the glass to the surrounding air, is denoted as h_1 , can be determined by employing (10).²¹

$$h_1 = 2.8 + 3V. \quad (10)$$

The variable V represents the velocity of air.

The radiation heat loss from glass to the surrounding air can be determined through the utilization of (11).

$$h_2 = \varepsilon_g \sigma \frac{[(T_g + 273)^4 - (T_{\text{sky}} + 273)^4]}{T_g - T_a}. \quad (11)$$

The temperature of the glass is denoted as T_g , while the temperature of the sky is denoted as T_{sky} . The glass emissivity coefficient is represented by ε_g , and Stefan's constant ($\sigma = 5.67 \times 10^{-8} \text{W/m}^2 \text{K}^4$) is utilized in the calculations, while

$$T_{\text{sky}} = T_a - 6.$$

Equation 12 can be utilized to calculate the convective heat losses from the absorber plate to the glass cover.²¹

$$h_3 = \frac{N_u k_{\text{ab}}}{d}. \quad (12)$$

The variable k_{ab} represents the thermal conductivity of the air gap, whereas the variable (d) denotes the distance of the air gap.

The Nusselt number of the air gap is denoted as N_u , can be determined by employing the next equation.²⁰

$$N_u = 1 + 1.44 \left[1 - \frac{1708}{R_a \cos \beta} \right]^+ \left(1 - \frac{\sin(1.8\beta)^{1.6} \times 1708}{R_a \cos \beta} \right) + \left[\left\{ \frac{R_a \cos \beta}{5830} \right\}^{\frac{1}{3}} - 1 \right]^+ . \quad (13)$$

The Rayleigh number denoted as R_a , can be determined by employing (14), whereas β represents the inclination of the collector angle.²¹

$$R_a = \frac{g \beta \Delta T d^3}{\nu \alpha_a}, \quad (14)$$

$$\beta = \frac{2}{(T_p + T_g)}.$$

In this context, the symbol g represents the acceleration due to gravity, while ΔT denotes the temperature difference between the plate and the glass. The symbol ν represents the kinematic viscosity, and α_a represents the thermal diffusivity.

The calculation of heat loss from the absorber plate to the glass cover through radiation can be determined by employing Eq. (15).²¹

$$h_4 = \varepsilon_{\text{eff}} \sigma \frac{[(T_p + 273)^4 - (T_g + 273)^4]}{T_p - T_g}. \quad (15)$$

The effective emissivity of the absorber plate and glass cover, denoted as ε_{eff} , can be determined by utilizing Eq. (16).

$$\varepsilon_{\text{eff}} = \left[\frac{1}{\varepsilon_p} + \frac{1}{\varepsilon_g} - 1 \right]^{-1}. \quad (16)$$

The symbol ε_p represents the effective emissivity of the plate, while ε_g denotes the effective emissivity of the glass.

The calculation of heat loss from glass to the surrounding environment through heat conduction can be determined using (17).²¹

$$h_5 = \frac{k_g}{L_g}. \quad (17)$$

In this context, the symbol k_g represents the thermal conductivity of the glass material, while L_g denotes the thickness of the glass.

Bottom loss coefficient (U_b)

Equation (18) can be utilized for the computation of the coefficient of bottom loss.²¹

$$U_b = \left[\frac{1}{h_7} + \frac{1}{h_1 + h_6} \right]^{-1}. \quad (18)$$

The heat loss (h_6) from the plate to the ambient through the insulation, caused by heat radiation, can be determined by utilizing Eq. (19).

$$h_6 = \varepsilon_i \sigma \frac{[(T_i + 273)^4 - (T_{\text{sky}} + 273)^4]}{T_i - T_a}. \quad (19)$$

The insulation emissivity, denoted as ε_i , is a variable of interest in this context.

The heat loss, denoted as h_7 , resulting from heat conduction through the insulation material can be determined by employing (20)

$$h_7 = \frac{k_i}{L_i}. \quad (20)$$

The variable k_i represents the thermal conductivity of the insulation, while L_i denotes the thickness of the insulation.

Edge loss coefficient (U_E)

The calculation of heat loss through the edge of the collector can be determined by employing (21).²¹

$$U_E = U_b \left(\frac{A_e}{A} \right). \quad (21)$$

The variable A_e represents the area of the collector edge, whereas A represents the area of the collector.

Materials and methods

The production of the copper tubing utilized in the construction of the spiral collector posed difficulties owing to its intricate configuration, necessitating the use of specialized

bending apparatus. As a result, the tubing was produced within the industrial workshops located in Duhok, utilizing the aforementioned equipment. The experiment was carried out in Duhok City over multiple days spanning the year 2022. The data collected by the collector was obtained through the utilization of a data logger, which was subjected to diverse weather conditions.

The collector was installed at a 37° angle facing south following the latitude of Duhok, as depicted in Fig. 2. The collector plays a vital role in the solar water heating system as it is responsible for the acquisition of solar radiation and subsequent conversion into thermal energy, which is utilized to heat the fluid flowing through the tubes. In the context of this investigation, the spiral collector was subjected to examination. The choice of copper as a material was based on its superior flexibility in comparison to steel, as well as its enhanced thermal conductivity when compared to steel tubes.

The copper tube utilized for the collector had a suitable outer diameter of 9.52 mm and a thickness of 0.71 mm. The total length of the tube employed for the collector amounted to 7.8 m. Table 1 presents the characteristics of the collector.

The Autodesk Inventor software was utilized to accurately calculate the dimensions of the collector, as depicted in Fig. 3. The measurements are in millimeters. The solar collector collected heated water, which was subsequently stored in a 60-L insulated tank, as depicted in Fig. 4. To reduce heat loss, the storage tank was adequately insulated.

The water was introduced into the spiral collector through its lower section and discharged through the upper section, as depicted in Fig. 5. To quantify the temperature of different components within the system, three distinct types of temperature sensors were employed. The temperatures of the plate, glass cover, and air gap were measured using K-Type thermocouples. The researchers utilized Waterproof Ds18B20 temperature sensors to assess the temperature of the water at both the inlet and outlet points of the collector. The ambient temperature was measured using a Temperature Sensor LM35 and a thermometer. Furthermore, a flow meter sensor was employed to quantify the flow rate of the water being introduced into the collector. To facilitate the logging and recording of data obtained during the experiment, a data logger was employed, specifically an Arduino Mega microcontroller.

The measurement of solar irradiance was conducted using an SM206 solar power meter. The device possesses the ability to quantify solar irradiance within a specified range of 1-3999 W. It was positioned atop the collector, as depicted in Fig. 6. The solar power meter was positioned at an identical angle to the collector, Ref. 22 recommendation.

Two anemometers were utilized to measure wind speed in the course of the experiment. The WH-SP-WS01 anemometer, depicted in Fig. 7 was employed in conjunction with the

Figure 2. Experimental setting of the spiral flow solar water heating system.

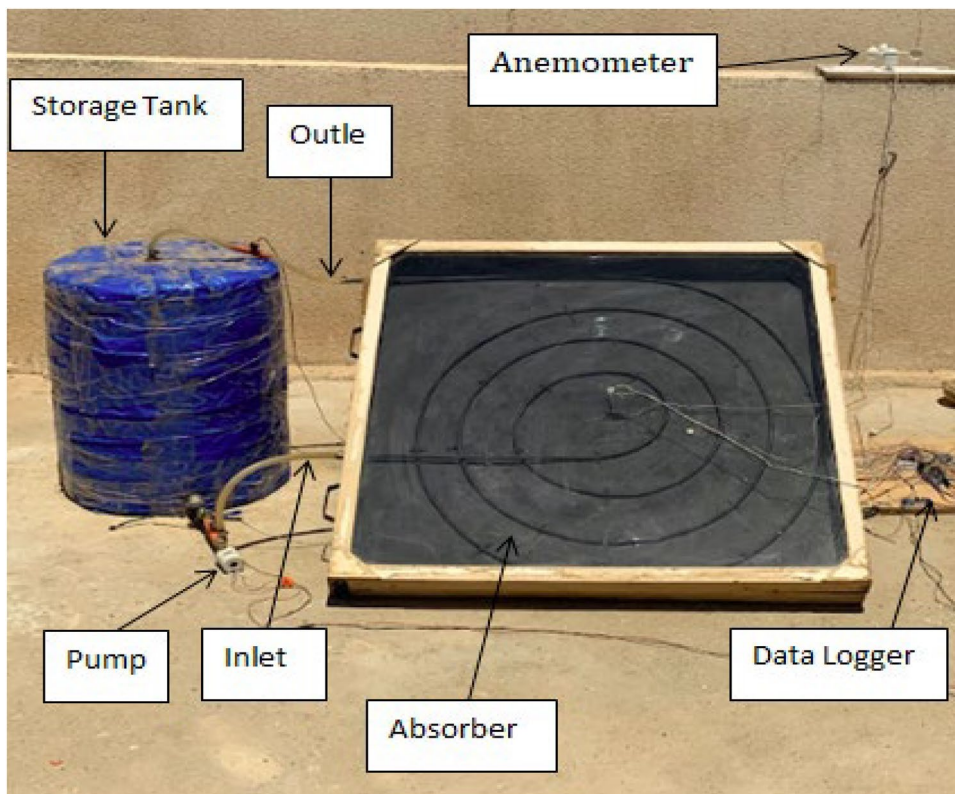


Table 1. The selected dimension and material properties of the utilized collector.

Item	Dimension	Material
Area of plate	1 m ²	Galvanized steel
Tube diameter	9.52 mm	Copper
Tube length	7.8 m	
Distance between tube	11 cm	
Air gap	8.5 cm	
Cover thickness	4 mm	Glass
Insulation thickness	2 cm	Wood

HP-866B digital anemometer, which is known for its higher level of accuracy.

Uncertainty analysis

To evaluate the precision of the experiment, a thorough analysis of uncertainties was performed, following the recommendation provided by Refs. 23 and 24. It is imperative to acknowledge that the devices employed in the experiment possess inherent measurement errors. The water mass flow rate sensor exhibits an error rate of approximately 1%. Similarly, the anemometer demonstrates an error rate of approximately 5%. Additionally, the solar irradiance meter displays an error rate of approximately 5%. Lastly, the thermocouples exhibit an error rate of approximately 0.5%.

The uncertainty of the collector efficiency was determined using Eq. (7),^{23,24} which incorporates the pertinent variables, such as the mass flow rate (\dot{m}), solar irradiance (W_s), temperature difference (ΔT), and irradiance angle (I). The calculation of the uncertainty in collector efficiency can be determined by employing Eq. (22).

Figure 3. The 2D shape and dimension for the utilized collector.

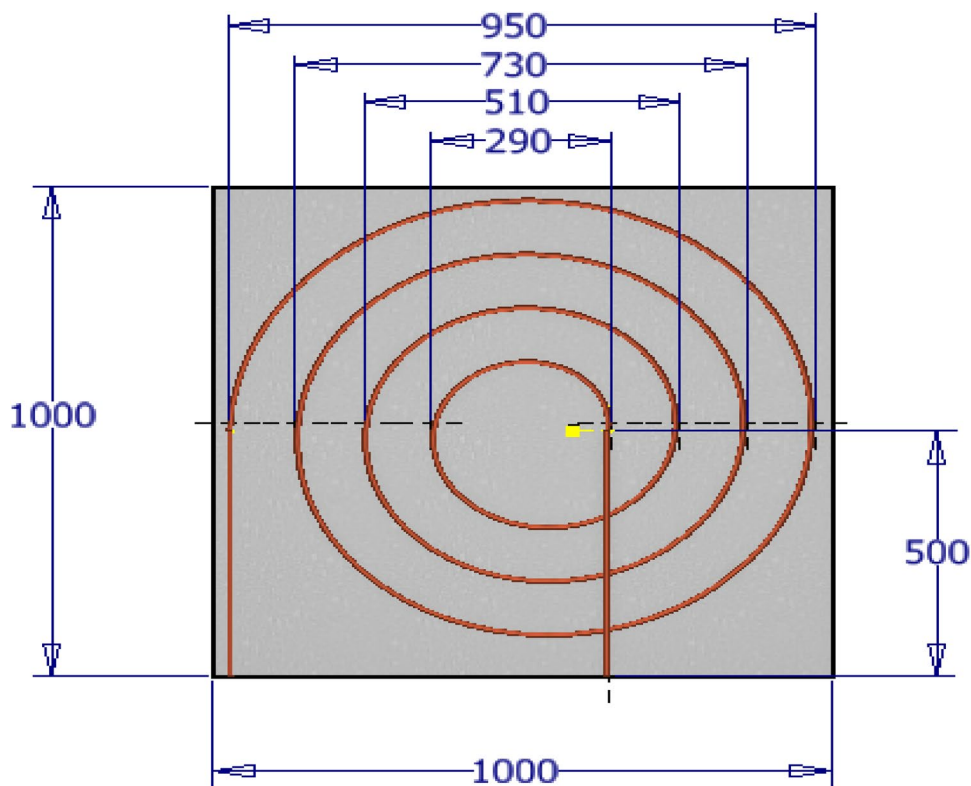


Figure 4. Insulated storage tank utilized in the experimental work.



$$\omega_{\eta} = \left[\left(\frac{\Delta \dot{m}}{\dot{m}} \right)^2 + \left(\frac{\Delta W_S}{W_S} \right)^2 + \left(\frac{\Delta I}{I} \right)^2 + \left(\frac{\Delta(T_o - T_i)}{(T_o - T_i)} \right)^2 \right]^{\frac{1}{2}}$$

$$\omega_{\eta} = \left[(0.01)^2 + (0.05)^2 + (0.05)^2 + (0.005)^2 \right]^{\frac{1}{2}}$$

$$\omega_{\eta} = [0.005125]^{\frac{1}{2}}$$

$$\omega_{\eta} = 0.0716$$

$$\omega_{\eta} = 7.16\%.$$

(22)

Results and discussion

This section presents the results achieved during the current work and tries to significantly and accurately discuss them through relationships that were drawn and presented using Microsoft Excel sheets. It also highlights the influences of the investigated parameters, such as wind speed and solar irradiance values, on the exit water temperature and the amount of energy gained at various values of water mass flow rate. The

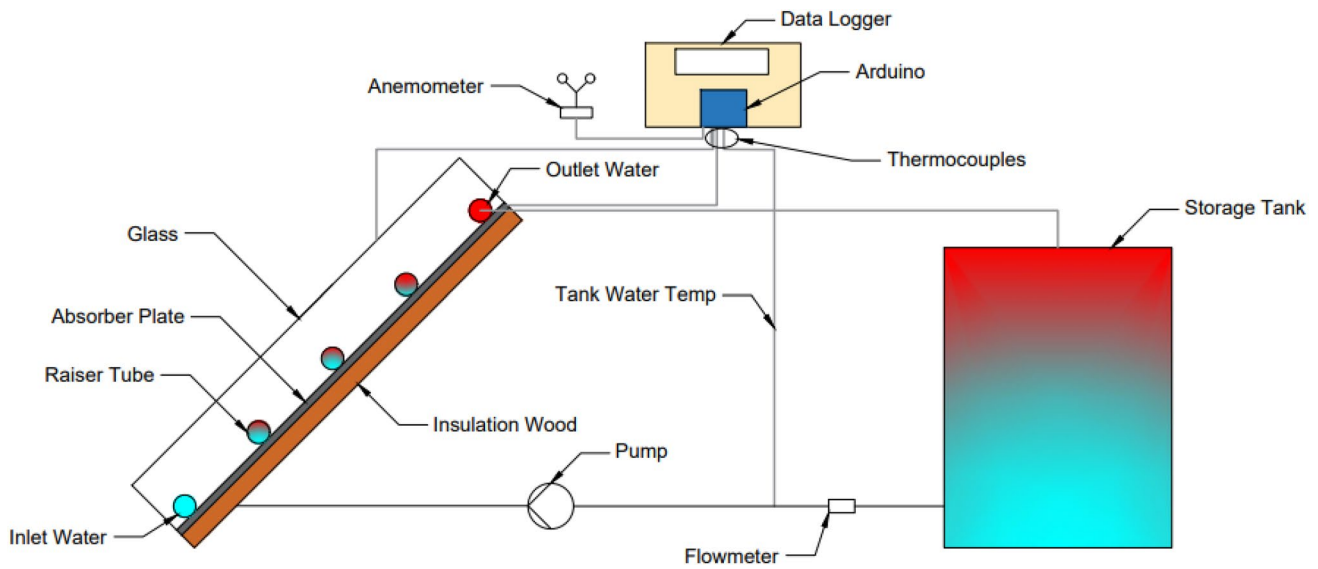


Figure 5. Illustration of a solar water heater.



Figure 6. Solar irradiance meter utilized during the experimental work.

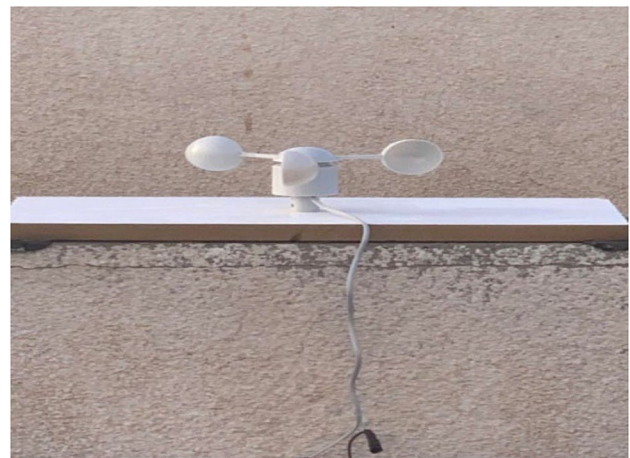


Figure 7. Wind speed meter utilized during the experimental work.

equations required to calculate the thermal collector efficiency and associated variables were solved using a Matlab program. The program accounted for the error rates of the devices and measurements mentioned earlier. The outcomes were observed during two distinct months and encompassed six varied mass flow rates. The forthcoming presentation will encompass a comprehensive analysis of the entirety of data gathered throughout the experimental process.

Figure 8a illustrates the temperature measurements obtained from the initial and concluding water tanks of the spiral collector. As anticipated, there was a positive correlation between solar irradiance and the temperature rise. The maximum temperature of the water tank in the spiral collectors was observed at a flow rate of 0.05 kg/s. It is observable and evident from the analysis

conducted that the spiral collector exhibited a level of performance that can be deemed satisfactory when subjected to testing across a spectrum of different flow rate values. The results obtained from the tests indicate that the spiral collector was able to consistently deliver adequate performance levels under varying flow conditions.

Figure 8b depicts the variations in temperature for the glass cover, plate absorber, air gap, and ambient temperature within the spiral collector, with respect to the mass flow rate and solar irradiance. The data clearly demonstrate that the temperature of both the glass cover and plate absorber exhibited a positive correlation with the intensity of solar radiation. The temperatures of the glass cover, plate absorber, and air gap in the spiral collectors attain their maximum values when the flow rate was 0.05 kg/s. It is noteworthy that the ambient temperature within the spiral collectors attains its maximum value of 38.6 °C when the flow rate is 0.42 kg/s. This finding deviates from the observed pattern

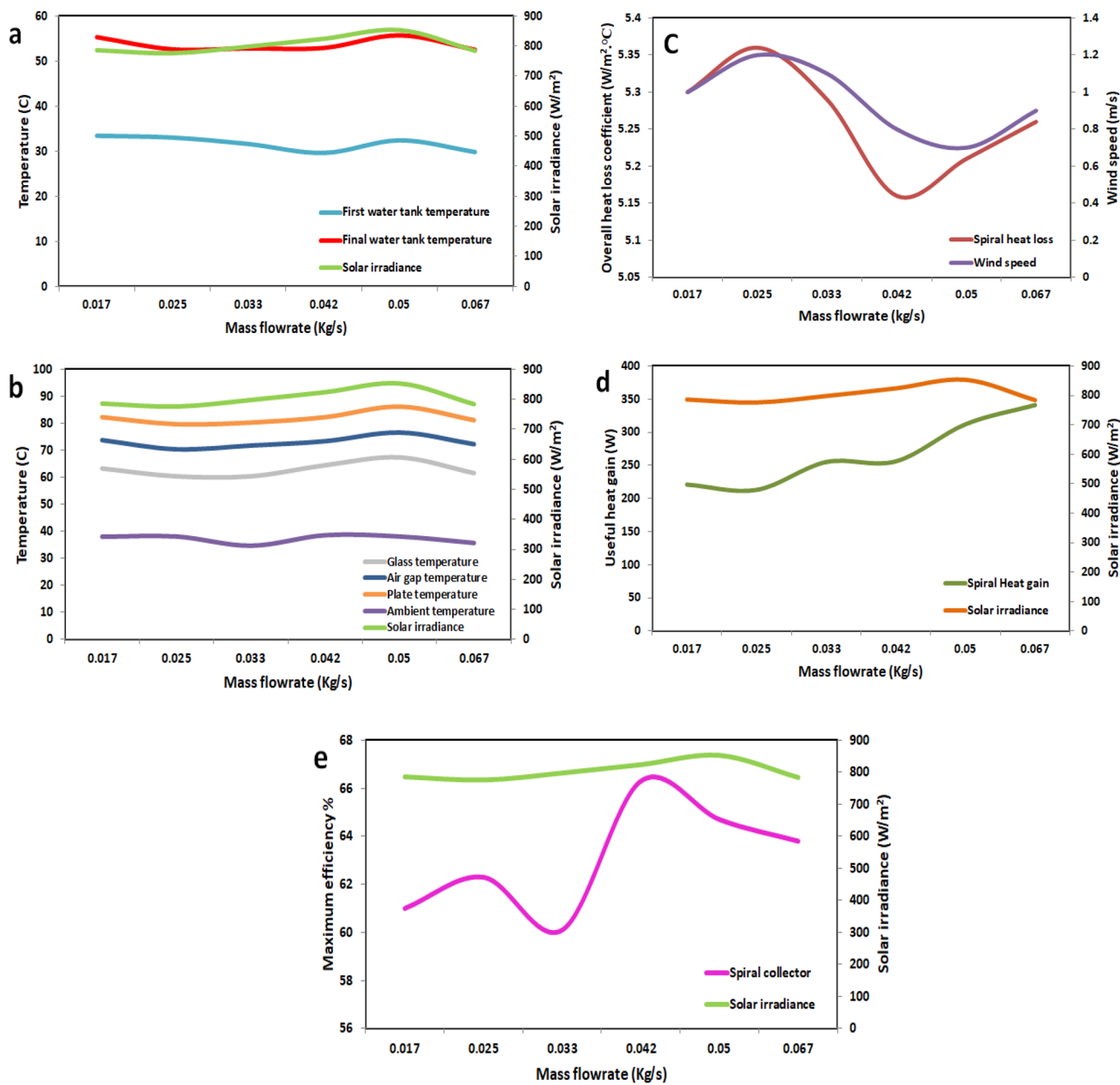


Figure 8. Spiral flow collector results. (a) The temperature of a solar water heater tank is influenced by solar radiation and the mass flow rate, (b) the temperature of a solar collector is influenced by solar radiation and the mass flow rate, (c) the effect of wind speed on the thermal heating capacity of the solar collector, (d) solar radiation and water flow rate influence on a solar collector's thermal output, and (e) the mass flow rate effect on solar collector efficiency.

for the remaining temperatures. The efficiency of the spiral collector in the process of capturing and transforming solar radiation into thermal energy is evidently apparent. This assertion is substantiated by the noticeable elevation in temperatures experienced by both the glass cover and plate absorber with the escalation of solar irradiance. The empirical evidence underscores the effectiveness of the spiral collector in harnessing solar energy and converting it into a usable form of heat.

Figure 8c illustrates the relationship between wind speed and the overall heat loss coefficient. As the wind speed

increases, there is a corresponding increase in the overall heat loss coefficient. The maximum overall heat loss coefficient was recorded at a wind velocity of 1.2 m/s and a mass flow rate of 0.025 kg/s, yielding a magnitude of 5.36 W/m² °C. This implies that fluctuations in the velocity of air movement possess a significant impact on the comprehensive coefficient governing the dissipation of heat in the tubular absorber. To be more precise, heightened levels of wind speed are directly correlated with increased rates of heat dispersal across the surface of the collector.

Figure 8d illustrates the fluctuation in the useful heat gain of the spiral collector. In general, the useful heat gain exhibited satisfactory performance across all mass flow rate values. The highest effective heat gain was observed when the mass flow rate was 0.067 kg/s. The findings of this study indicate that the spiral collector exhibits efficacy in capturing and converting solar radiation into heat energy that can be utilized effectively. Moreover, it is observed that higher mass flow rates are associated with increased useful heat gains.

Figure 8e depicts the fluctuating efficiency of the spiral collector, which is influenced by variations in both the mass flow rate and solar irradiance. The performance of the spiral collector was observed to be satisfactory when evaluated across a range of mass flow rate values. Specifically, the spiral collector exhibited exceptional efficiency when operating at a mass flow rate of 0.042 kg/s, thereby highlighting its superior performance relative to the various other mass flow rate values that were tested in the study.

The findings of this study suggest that the spiral collector demonstrates efficacy in the capture and conversion of solar radiation into thermal energy. Furthermore, it is observed that enhancing the mass flow rate can result in improved efficiency. Researchers, engineers, and individuals with a vested interest in technological advancements are strongly encouraged to persist in their efforts to enhance, develop, produce, and employ this novel form of straightforward, economical, and efficient technology.

Conclusion

Based on the conducted experiments, it can be inferred that the spiral collector exhibited favorable performance, wherein an increase in solar irradiance resulted in enhanced performance. The performance of the collector was influenced by various factors, such as solar irradiance, wind speed, and mass flow rate.

The results yield several key points that can be inferred.

- The spiral collector demonstrated optimal efficiency when operated at a flow rate of 0.042 kg/s, resulting in a peak efficiency of 66.3%.
- The highest recorded temperature increase in the water tank occurred at mass flow rates of 0.042 and 0.05 kg/s, resulting in a temperature rise of 23.3 °C in the year 2022.
- The highest recorded heat gains that were deemed beneficial occurred at a mass flow rate of 0.067 kg/s, resulting in a value of 505 W.
- The efficiency of the thermal collector was negatively affected by wind speed, as higher wind speeds resulted in an increase in the heat loss coefficient and a decrease in overall efficiency.
- The highest overall heat loss coefficient was recorded at a mass flow rate of 0.025 kg/s, yielding a value of 5.36 W/m² °C.

The present investigation illustrated that spiral collectors have the potential to function as a feasible alternative for fuel and energy in domestic environments. This allows inhabitants in our locality to build and employ this straightforward design of collector, thus deriving advantages from its use.

In general, the findings of this study indicate that enhancing the design and functioning of the spiral collector can result in enhanced performance. Moreover, it is crucial to carefully evaluate factors such as solar irradiance, wind speed, and mass flow rate to attain efficient and effective energy conversion.

Acknowledgments

The authors would like to thank the University of Zakho and the University of Mosul for supporting this work.

Author contributions

Ahmed Abdulsitar contributed to analysis and writing original manuscript. Nofal Hasan contributed to conceptualization, methodology, and supervision. Ali Basem contributed to editing and writing—final manuscript. Ahmed Daabo contributed to reviewing and writing final manuscript. Abdulelah Yaseen contributed to reviewing and editing—original draft. Hudhaifa Hamzah contributed to reviewing—final manuscript.

Funding

Authors state no funding involved.

Data availability

Some or all data, models, or code that support the findings of this study are available from the corresponding author upon reasonable request.

Declarations

Competing interests

The authors declare that they have no known competing financial or personal relationships that could have influenced the work reported in this paper.

REFERENCES

1. M.D. Sarmouk, A. Smaili, A. Merabtine et al., Experimental development of a hybrid solar-gas heating system. *MRS Energy Sustain.* **8**, 110–117 (2021). <https://doi.org/10.1557/s43581-021-00007-7>
2. M.A. Bashir, A.M. Daabo, K.P. Amber, M.S. Khan, A. Arshad, H. Elahi, Effect of phase change materials on the short-term thermal storage in the solar receiver of dish-micro gas turbine systems: a numerical analysis. *Appl. Therm. Eng.* **195**, 117179 (2021). <https://doi.org/10.1016/j.applthermaleng.2021.117179>
3. A.M. Daabo, K.E. Hammo, O.A. Mohammed, A.A. Hassan, T. Lattimore, Performance investigation and design optimization of micro scale compressed air axial turbine for domestic solar

- powered Brayton cycle. *Sustain. Energy Technol. Assess.* **37**, 100583 (2020)
4. K. Patel, P. Patel, J. Patel, Review of solar water heating systems. *Int. J. Adv. Eng. Technol.* **E 3**(4), 146–149 (2012)
 5. D. Balamurali, M. Natarajan, Numerical-experimental analysis of solar liquid flat-plate collector with different HTF and internal grooves profiles in the absorber duct. *Appl. Sol. Energy* **59**, 244–252 (2023). <https://doi.org/10.3103/S0003701X21101175>
 6. R.D. Salim, Design and improving the work of a concave solar collector-CSC. *Period. Eng. Nat. Sci.* **8**(3), 1471–1481 (2020)
 7. S. Jebaraj, S. Iniyan, A review of energy models. *Renew. Sustain. Energy Rev.* **10**(4), 281–311 (2006)
 8. T.M. Letcher, V.M. Fthenakis, *A Comprehensive Guide to Solar Energy Systems: With Special Focus on Photovoltaic Systems* (Academic Press, New York, 2018)
 9. P. Li, T. Liu, Y. Qin et al., Performance enhancement of parabolic trough collector by using homogenizer and spiral. *J. Therm. Sci.* **33**, 658–674 (2024). <https://doi.org/10.1007/s11630-024-1943-y>
 10. A.M. Daabo, E. Bellos, S. Pavlovic, M.A. Bashir, S. Mahmoud, R.K. Al-Dadah, Characterization of a micro thermal cavity receiver—experimental and analytical investigation. *Therm. Sci. Eng. Prog.* **18**, 100554 (2020). <https://doi.org/10.1016/j.tsep.2020.100554>
 11. K.F. Nasir, Thermal Performance of Plastic Receiver in Solar Collector. *J. Eng.* **25**(7), 37–60 (2019). <https://doi.org/10.31026/j.eng.2019.07.03>
 12. S. Singh, K. Mausam, S.K. Ghosh et al., An experimental and numerical approach for thermal performance investigation of solar flat plate collector. *Environ. Sci. Pollut. Res.* **30**, 92859–92879 (2023). <https://doi.org/10.1007/s11356-023-28843-9>
 13. A.E.M. Fodah, T.A.M. Abdelwahab, K.A.M. Ali et al., Performance evaluation of solar photovoltaic panels under bird droppings accumulation using thermography. *MRS Energy Sustain.* (2024). <https://doi.org/10.1557/s43581-024-00081-7>
 14. H.S. Hamood, B.M. Salim, N.M. Abdulrazzaq, Theoretical analysis of flat plate solar collector placed in Mosul city by using different absorbing materials and fluids. *Kufa J. Eng.* (2015). <https://doi.org/10.30572/2018/KJE/621152>
 15. R.D. Maldonado, E. Huerta, J.E. Corona, O. Ceh, A.I. Leon, I. Henandez, Design and construction of a solar flat collector for social housing in México. *Energy Procedia* **57**, 2159–2166 (2014)
 16. R. Bakari, R.J.A. Minja, K.N. Njau, Effect of glass thickness on performance of flat plate solar collectors for fruits drying. *J. Energy* **2014**, 1–8 (2014). <https://doi.org/10.1155/2014/247287>
 17. A. Kleivinskas, V. Bučinskas, Analysis of a flat-plate solar collector. *Moksl. Liet. ateitis* **3**, 39–43 (2011)
 18. G.N. Tiwari, A. Tiwari, Shyam, in *Handbook of Solar Energy: Theory, Analysis and Applications*, ed. by G.N. Tiwari, A. Tiwari, Shyam (Springer, Singapore, 2016), pp. 327–368. <https://doi.org/10.1007/978-981-10-0807-8>
 19. A.M. Daabo, S. Zubeer, H. Ismaeel, F. Mustafa, H. Hamzah, A. Basem, H. Easa, A novel economic and technical dispatch model for household photovoltaic system considering energy storage system in “Duhok” City/Iraq as a case study. *J. Energy Storage* **94**, 112440 (2024)
 20. A.M. Daabo, A.A. Hassan, M.A. Bashir, H. Hamza, S. Salim, A. Koprulu, T. Badawy, S. Mahmoud, R. Al-Dadah, Experimental study and 3D optimization of small-scale solar-powered radial turbine using 3D Printing technology. *Machines* **11**(8), 817 (2023)
 21. A.M. Daabo, S. Mahmoud, R.K. Al-Dadah, Structural analysis of small scale radial turbine for solar powered Brayton cycle application, in *ASME 2018 12th International Conference on Energy Sustainability collocated with the ASME 2018 Power Conference and the ASME 2018 Nuclear Forum*, vol. 51418 (American Society of Mechanical Engineers, 2018)
 22. T.A. Yassen, N.D. Mokhlif, M.A. Eleiwi, Performance investigation of an integrated solar water heater with corrugated absorber surface for domestic use. *Renew. Energy* **138**, 852–860 (2019). <https://doi.org/10.1016/j.renene.2019.01.114>
 23. A. Alkhabbaz, H. Hamza, A.M. Daabo, H.-S. Yang, M. Yoon, A. Koprulu, Y.-H. Lee, The aero-hydrodynamic interference impact on the NREL 5-MW floating wind turbine experiencing surge motion. *Ocean Eng.* **295**, 116970 (2024)
 24. A. Noghrehabadi, E. Hajidavaloo, M. Moravej, Experimental investigation of efficiency of square flat-plate solar collector using SiO₂/water nanofluid. *Case Stud. Therm. Eng.* **8**, 378–386 (2016). <https://doi.org/10.1016/j.csite.2016.08.006>

Publisher's Note Springer Nature remains neutral with regard to jurisdictional claims in published maps and institutional affiliations.

Springer Nature or its licensor (e.g. a society or other partner) holds exclusive rights to this article under a publishing agreement with the author(s) or other rightsholder(s); author self-archiving of the accepted manuscript version of this article is solely governed by the terms of such publishing agreement and applicable law.